JOURNAL OF AIRCRAFT
Vol. 48, No. 1, January–February 2011

Study of the Reverse Delta Wing

Afaq Altaf,* Ashraf A. Omar,† Waqar Asrar,‡ and Hani Bin Ludin Jamaluddin*
International Islamic University Malaysia, Kuala Lumpur 50728, Malaysia

DOI: 10.2514/1.C031101

Particle image velocimetry was used in a low-speed wind tunnel to investigate the vortex structures of a slender reverse delta wing at various angles of attack and roll. This work investigates the characteristics of the vortices generated downstream in planes perpendicular to the freestream direction and their dependence on angles of attack and roll at a chord-based Reynolds number of $Re_c = 3.82 \times 10^5$. The peak tangential velocities at $\alpha > 5°$ show a trend similar to a delta wing. A six-component balance was used to obtain the aerodynamic coefficients for a reverse delta wing as well as a delta wing for comparison. A simulation of the streamlines, velocity vectors, and surface pressure contours was carried out using computational fluid dynamics software to show the characteristics of the flow over a reverse delta wing.

Nomenclature

C_D	=	drag coefficient
C_L	=	lift coefficient
C_m	=	moment coefficient
c	=	chord length, m
k	=	number of points
L/D	=	lift-to-drag ratio
Re_c	=	Reynolds number based on chord
r	=	radius, m
r_c	=	core radius, m
V_θ	=	tangential velocity, m/s
V_∞	=	freestream velocity, m/s
x	=	streamwise coordinate, m
y	=	spanwise coordinate, m
z	=	transverse coordinate, m
α	=	angle of attack, deg
Γ	=	circulation, m^2/s
ϕ	=	roll angle, deg

I. Introduction

THE purpose of this paper is to investigate the flow over a reverse delta wing. Reverse delta wings may be used in vortex alleviation [1]. They may also be used in forward-swept-winged aircraft [2].

Vortex flows play a vital role in modern aerodynamic applications such as in the control of wingtip vortices of large aircraft so as to minimize the hazard posed by trailing aircraft from such wake-vortex encounters [1,2].

Vortices created by aircraft are an inevitable consequence of the creation of lift. Vortices persist for many miles, and wake-vortex encounters pose a grave hazard to trailing aircraft that fly in close proximity near the airport runway, especially during takeoff and landing [3], because the tip vortex circulation is at a maximum. This limits the spacing between aircraft within the takeoff and landing corridors at busy airports and hence increases the time intervals between consecutive landings and takeoffs [4].

Received 7 May 2010; revision received 12 August 2010; accepted for publication 20 August 2010.

*Research Assistant, Department of Mechanical Engineering, Gombak, P.O. Box 10.

†Professor, Department of Mechanical Engineering, Gombak, P.O. Box 10. Member AIAA.

‡Professor, Department of Mechanical Engineering, Gombak, P.O. Box 10.

Worldwide research has been focused on increasing airport capacity by minimizing the wake-vortex hazard. The studies of forward-swept wings, which resemble a reverse delta wing, have shown promising results. Interest in forward-swept-wing aircraft is growing. The aerodynamics of a forward-swept wing shows that air moving over it tends to flow inward toward the root of the wing instead of outward toward the wingtip, as occurs on sweptback wings. This reverse airflow does not allow the wingtips and their ailerons to stall at high angles of attack. Both X-29 and Sukhoi Su-47 supersonic aircraft make use of forward-swept wings for superb maneuverability and operation at angles of attack up to 45 deg or more [5]. This type of configuration is made possible by lightweight nonmetallic composite materials that can withstand the increased amounts of aerodynamic forces. This configuration would provide a number of advantages, such as higher lift-to-drag ratio, higher capability in dogfight maneuvers, higher range at subsonic speed, improved stall resistance and antispin characteristics, improved stability at high angles of attack, a lower minimum flight speed, and shorter takeoff and landing distances [6].

A reverse delta wing has certain favorable aerodynamic characteristics that can be exploited for efficient supersonic flight. Early investigations into the aerodynamics of reverse delta wings were carried out by NACA in 1947 [7].

Gerhardt [7] has also studied the reverse delta wing at high Mach numbers and has observed significant differences between the regular delta wing and a reverse delta wing. According to his study, surface pressure contours of a reverse delta wing are expected to exhibit a more regular change in pressure than a delta wing and strong pressure gradients are expected to be confined to the trailing-edge regions.

In 1999, a group of Northrop Grumman designers came up with an innovative supersonic transport design incorporating an unusual reverse delta wing. Designers from Northrop Grumman claimed that, "The reverse delta wing design allows additional lift to be created at low speeds, reducing power requirements and therefore noise, during the environmentally crucial takeoff and landing phases" [8].

Recent investigations into the aerodynamics of a reverse delta wing were carried out by Elsayed et al. [9]. The vortex characteristics of the reverse delta wing showed promising results. Their investigation suggests that a reverse delta wing, as a wake alleviation add-on device, may excite some instability through stable laminar or unstable wave phase or through modifying the vortex roll-up process as a result of interaction with the turbulent phase. These can lead to rapid diffusion of vorticity, which can enhance wake-vortex decay and thus lead to wake-vortex alleviation.

A lot of research has been done on delta wings, especially on leading-edge vortex breakdown control [10], vortex bursting [11], simulation [12], and experimental and numerical investigation of delta wings [13]. Most of the research on delta wings has been performed using flow visualization and simulation to better understand

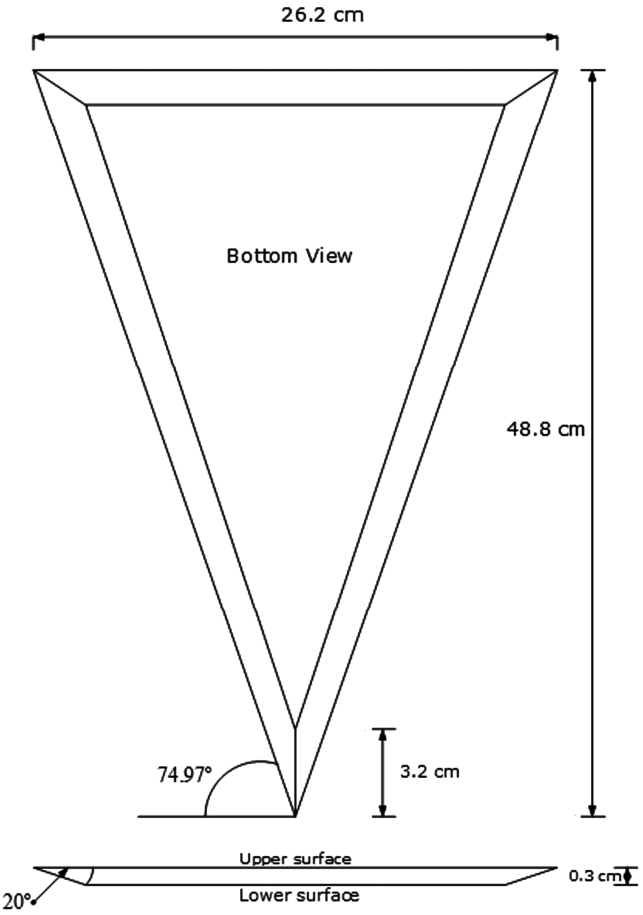

Fig. 1 Schematic of the wing model.

the flow characteristics over a delta wing. Some amount of research has been performed using particle image velocimetry (PIV), but the research is mostly concerning the leading-edge radius effects on delta wing flow [14]. There is very limited research performed that deals in detail with delta wing vortex characteristics using PIV. There seems to be very little or no published material on reverse delta wing vortex characteristics using PIV or using any other method. Hence, it was appropriate to conduct research in detail on reverse delta wing vortex characteristics at various angles of attack and roll using PIV.

PIV technique, a minimally intrusive method, is used in this work to study the vortex characteristics of a reverse delta wing at various angles of attack and roll. Vortex characteristics such as maximum tangential velocity, vorticity, and circulation distributions are presented, along with CFD simulation and six-component force balance results.

II. Experimental Setup

A. Wind Tunnel

The experiment was carried out in the closed-loop low-speed wind tunnel at the International Islamic University Malaysia (IIUM). The wind-tunnel test-section dimensions are 2.25 m (width), 1.5 m (height), and 6.0 m (length). The wind tunnel has a turbulence intensity of less than 0.11%. The model was placed in the test section by using a central strut.

B. Model

A reverse delta wing is bounded by a leading edge and by a pair of trailing edges extending from the ends of the leading edge toward a trailing apex point. As shown in Fig. 1, the reverse delta wing used in this investigation has a root chord of 488 mm, span of 262 mm, thickness of 3 mm, sweep angle of 74.97 deg , and bevel angle of 20 deg.

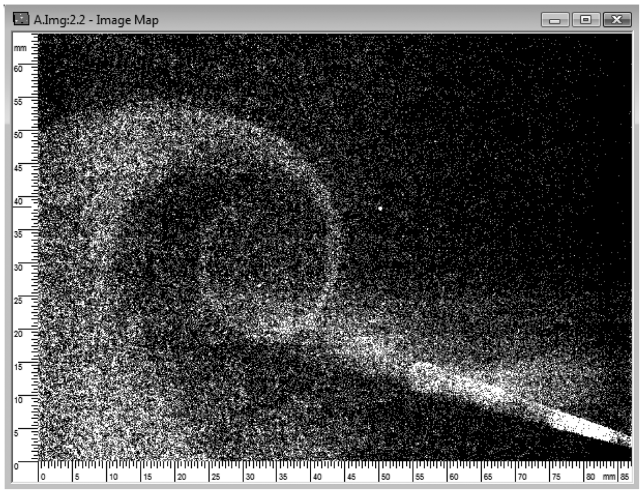

Fig. 3 PIV image map of the reverse delta wingtip vortex (left wingtip) at $\alpha = 5°$ and $\phi = 0°$.

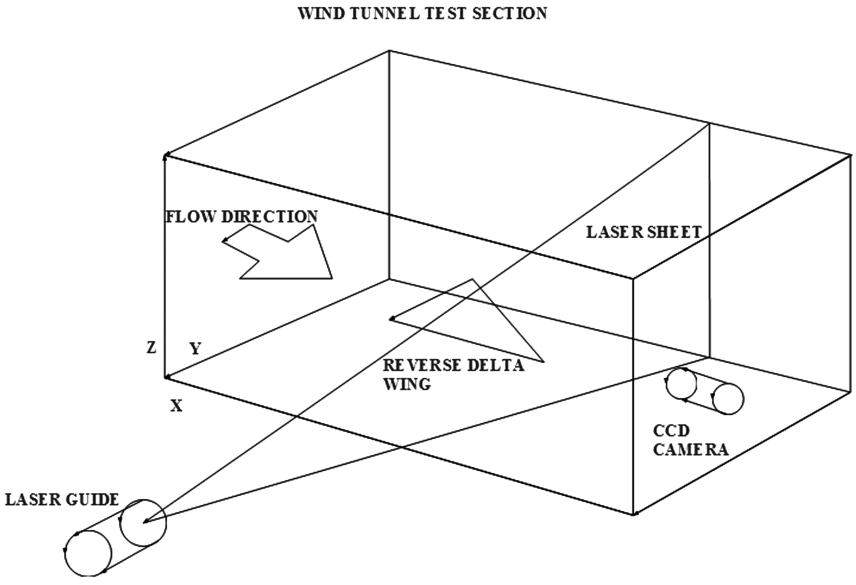

Fig. 2 Schematic of the experimental setup.

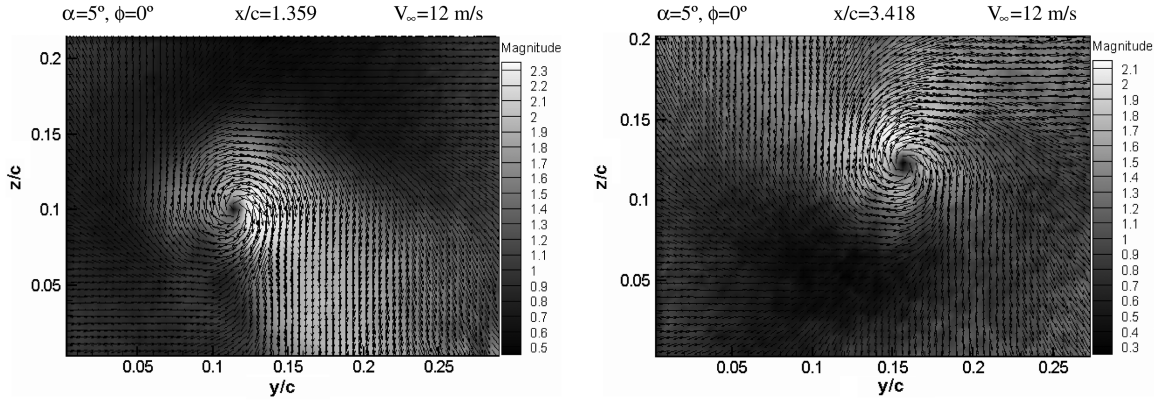

a) Reverse delta wing vortex at $\alpha=5^{o}$, $\phi=0^{o}$ and $Re_c=3.82\times10^5$

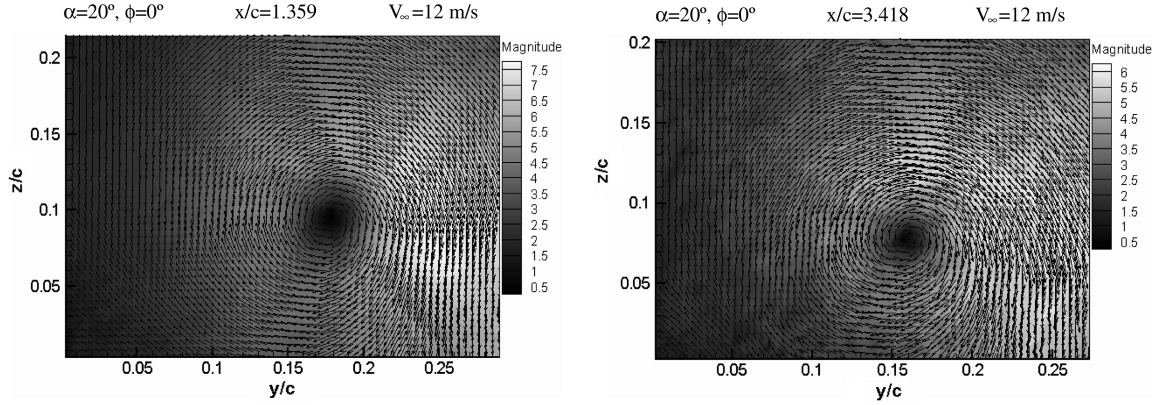

b) Reverse delta wing vortex at $\alpha=20^{o}$, $\phi=0^{o}$ and $Re_c=3.82\times10^5$

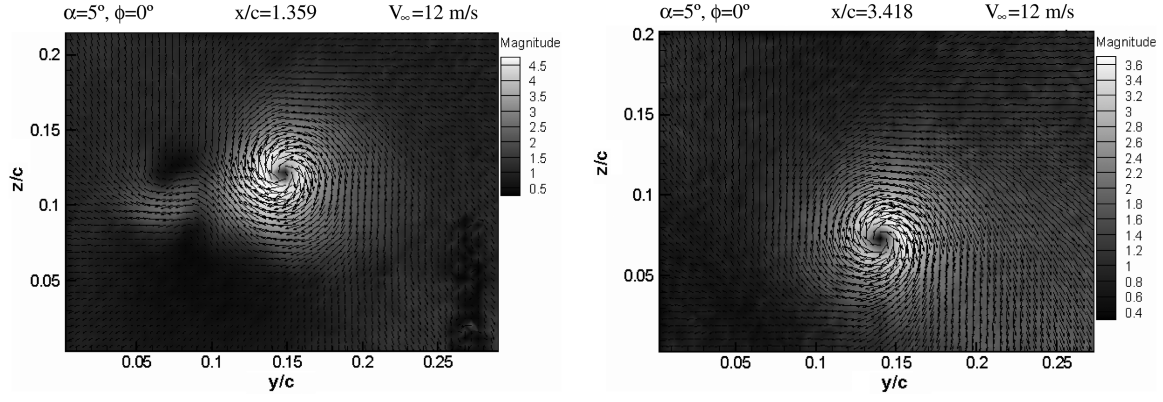

c) Regular delta wing vortex at $\alpha=5^{o}$, $\phi=0^{o}$ and $Re_c=3.82\times10^5$

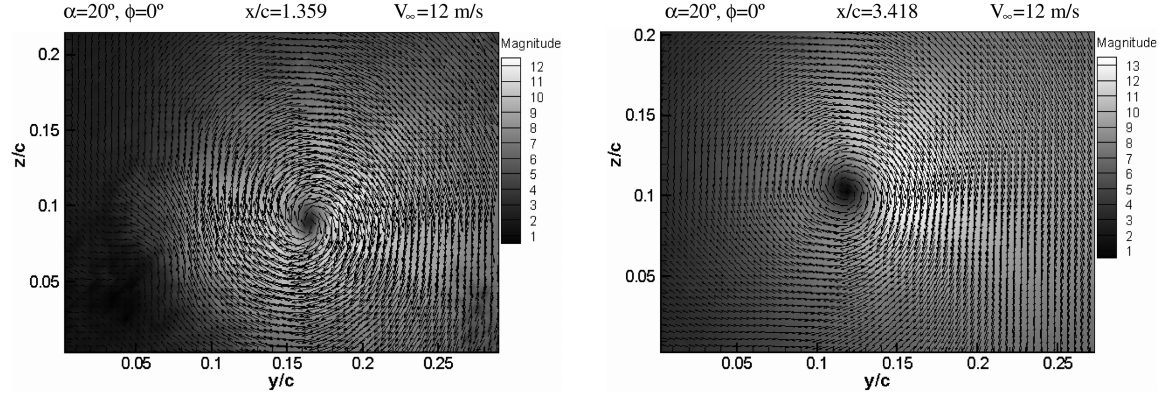

d) Regular delta wing vortex at $\alpha=20^{o}$, $\phi=0^{o}$ and $Re_c=3.82\times10^5$

Fig. 4 Wing tip vortex velocity vectors at various angles of attack at locations of $x/c = 1.359$ and 3.418 for a–b) reverse delta wing and c–d) regular delta wing.

A symmetrical airfoil was attached to the lower surface of the wing so that the wing could be easily mounted on to a movable joint, which in turn was mounted on to a strut in the wind-tunnel test section. The symmetrical airfoil was used to streamline the flow close to the wing body, because the movable joint and the circular strut have the tendency of creating their own wake.

Variations in the angle of attack and roll angles were made by using a movable joint. The angles were measured using an inclined-plane degree scale with an error of $\pm 1^\circ$.

C. Experimental Procedure

The velocity components in planes perpendicular to the streamwise direction at a location of $x/c = 1.359$ and 3.418 in the downstream direction are investigated. The experimental setup is shown in Fig. 2. Two laser positions are chosen so as to differentiate between their flow characteristics in terms of roll-up, tangential velocity, vorticity, and circulation.

The freestream velocity was set to 12 m/s corresponding to a $Re_c = 3.82 \times 10^5$. The flow was seeded by particles of a mean diameter of 1 μm. Important PIV data acquisition parameters such as time interval ($dt = 40$ μs) and laser-sheet thickness (3 mm) were fixed. A light sheet from a Nd:YAG laser system of wavelength 532 nm was used to illuminate the flow. A Flow Sense M2 8-bit charge-coupled-device (CCD) camera with Micro-Nikkor 60 mm camera lens was placed perpendicularly to the laser sheet, downstream of the wing.

Figure 3 shows an image map of a reverse delta wingtip vortex. The CCD camera is focused to view only the left wingtip vortex. PIV data were recorded for $\alpha = 5$, 10, 15, 20, and $\phi = 0^\circ$, ± 5 and $\pm 10^\circ$. Roll angle (ϕ) is considered positive when the right wing is lower than the left wing (clockwise) as seen by the camera. A total of 50 PIV images were recorded in each case and were postprocessed using adaptive correlation with a 25% overlap. The measurement resolution is 1600×1186 pixels. An initial interrogation area size of 256×256 pixels is used, which is reduced to a final interrogation area size of 32×32 pixels by making three refinement passes that yield 66×49 vectors per image.

The results were simple phase-averaged to estimate the mean velocity in the region of focus.

III. Results and Discussions

A. Velocity Vectors

Figures 4a and 4b show velocity vectors for a reverse delta wing (RDW) vortex, and Figs. 4c and 4d show velocity vectors for a delta wing (DW) vortex. The background of the figures corresponds to the tangential velocity, and the scale next to the figures shows the tangential velocity magnitude. The laser is positioned at locations of $x/c = 1.359$ and 3.418 for both the DW and the RDW.

In Fig. 4a, the RDW vortices exhibit a nonsymmetric shape, indicating that the tangential velocity is not sufficient for the vortices to roll up completely. In Fig. 4b, the RDW vortices exhibit an axisymmetric shape with better roll-up. It can be concluded that as the angle of attack increases the tangential velocity magnitude also increases, which results in better roll-up of the vortices.

In Fig. 4c, the DW vortices are seen to exhibit better roll-up than RDW vortices, shown in Fig. 4a, due to a higher tangential velocity magnitude. The vorticity contours shown in Figs. 5a and 5b also show that a DW vortex exhibits a better roll-up than an RDW vortex. The vortices in Figs. 4c and 4d exhibit an axisymmetric shape.

From Fig. 4d, the DW vortex at a location of $x/c = 3.418$ exhibits a slightly higher tangential velocity than at a location of $x/c = 1.359$, which can be due to the averaging of the PIV images. The region of highest tangential velocity magnitude of 13 m/s does not appear in the tangential velocity distribution because the exported data are arranged into specific ranges and then averaged to obtain a smooth distribution. Because of the averaging process, the tangential velocity distribution at a location of $x/c = 1.359$ still tends to exhibit a higher magnitude than that at a location of $x/c = 3.418$ downstream, as shown in Fig. 6d.

From Figs. 4a–4d, it can be concluded that the DW vortices exhibit a tangential velocity magnitude that is nearly twice that of the RDW vortices and that the DW and RDW vortices also exhibit better roll-up at locations farther downstream when the angle of attack increases.

As the angle of attack increases, the RDW and DW vortices gain sufficient tangential velocity to roll up. At a farther downstream location, the vortices get sufficient time to roll up, but at the same time they lose a fair amount of tangential velocity in an effort to travel a significant distance. The results yield a similar trend for RDW and DW vortices at various angles of attack and roll.

The uncertainty analysis was performed using the International Organization for Standardization procedure [15]. Based on 95%-confidence intervals, the total uncertainty in velocity was found to be ± 0.3336 m/s.

B. Vorticity Contours

The vorticity decreases gradually from a maximum at the center to nearly zero at the outer region of the RDW and DW vortices for all the cases investigated. As the angle of attack increases, the vorticity increases in magnitude, and a larger dimension and closer vorticity contours are recorded for all cases. At a particular angle of attack, a DW vortex exhibits a higher vorticity magnitude than an RDW vortex.

Figures 5a and 5b show the vorticity contours at $\alpha = 20^\circ$ and $\phi = 5^\circ$ for an RDW and a DW vortex, respectively. From the figures it can be noted that a DW vortex exhibits uniform spacing of vorticity contours nearly throughout the vortex core. Small patches of vorticity exist at the outer regions of the DW vortex, suggesting that the roll-up phase has not completed. An RDW vortex exhibits uniform spacing of vorticity contours only at the center of the vortex, whereas the outer region is fully occupied by smaller patches of vorticity, indicating that an RDW vortex takes longer to roll up than a DW vortex, mainly due to the lower tangential velocity magnitude exhibited by an RDW vortex.

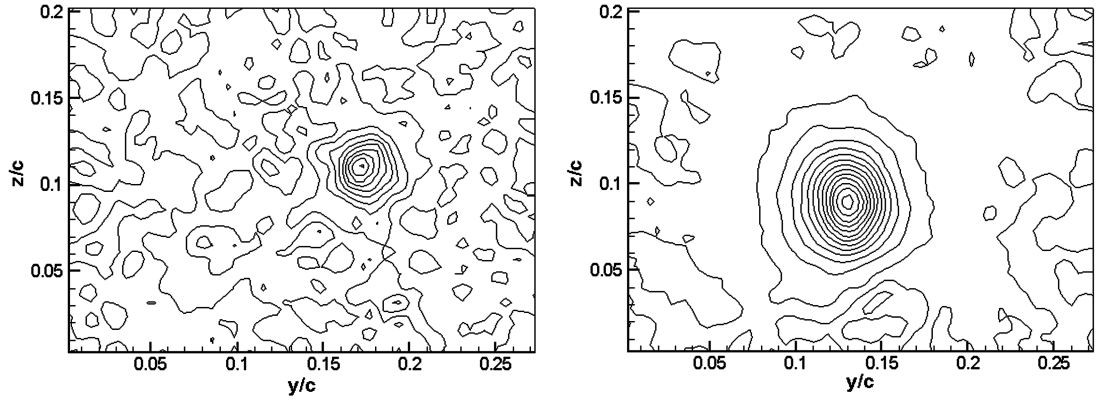

Fig. 5 Vorticity contour at $\alpha = 20^\circ$ and $\phi = 5^\circ$ at a location of $x/c = 3.418$ for a) reverse delta wing and b) regular delta wing.

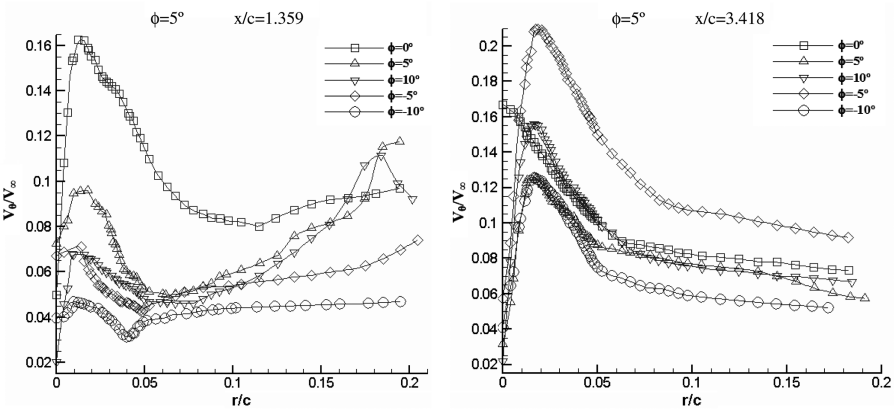

a) Tangential velocity distributions of a reverse delta wing at α=5°

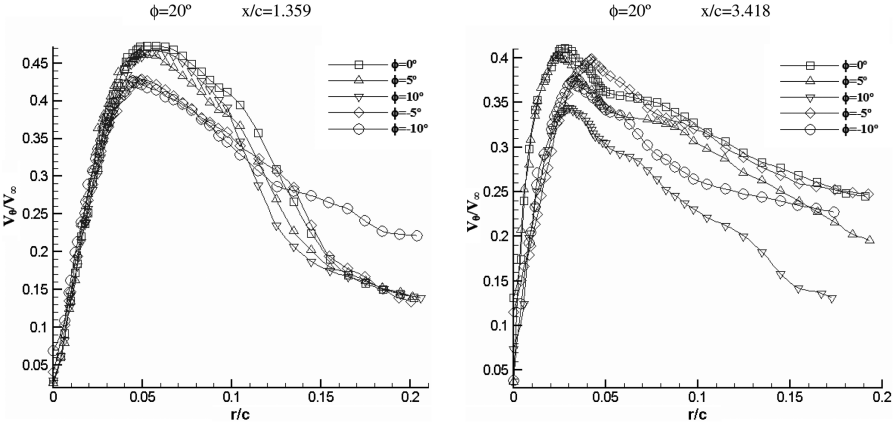

b) Tangential velocity distributions of a reverse delta wing at α=20°

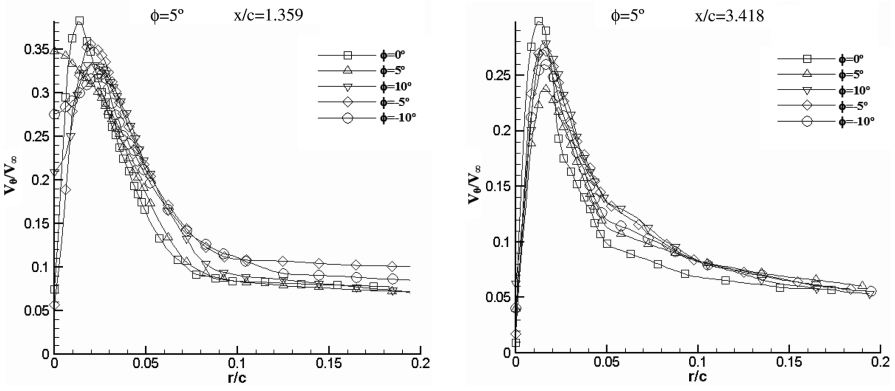

c) Tangential velocity distributions of a regular delta wing at α=5°

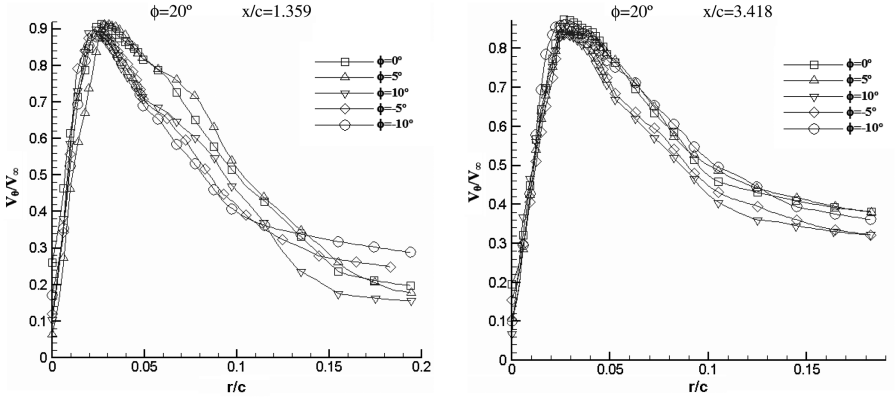

d) Tangential velocity distributions of a regular delta wing at α=20°

Fig. 6 Nondimensional tangential velocity of tip vortices at various angles of attack at locations of $x/c = 1.359$ and 3.418 for a–b) reverse delta wing and c–d) regular delta wing.

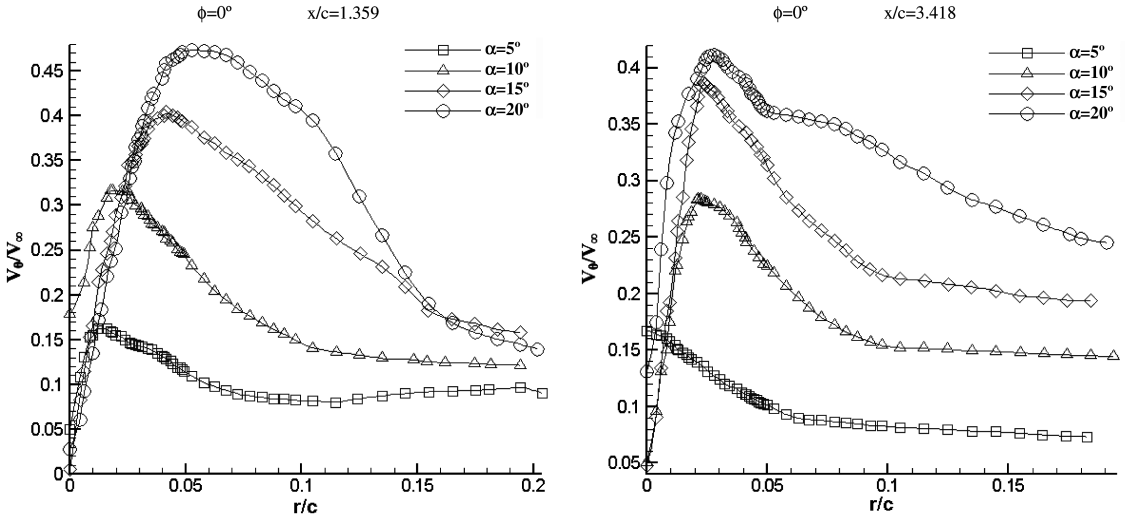

a) Tangential velocity distributions of a reverse delta wing at ϕ=0°

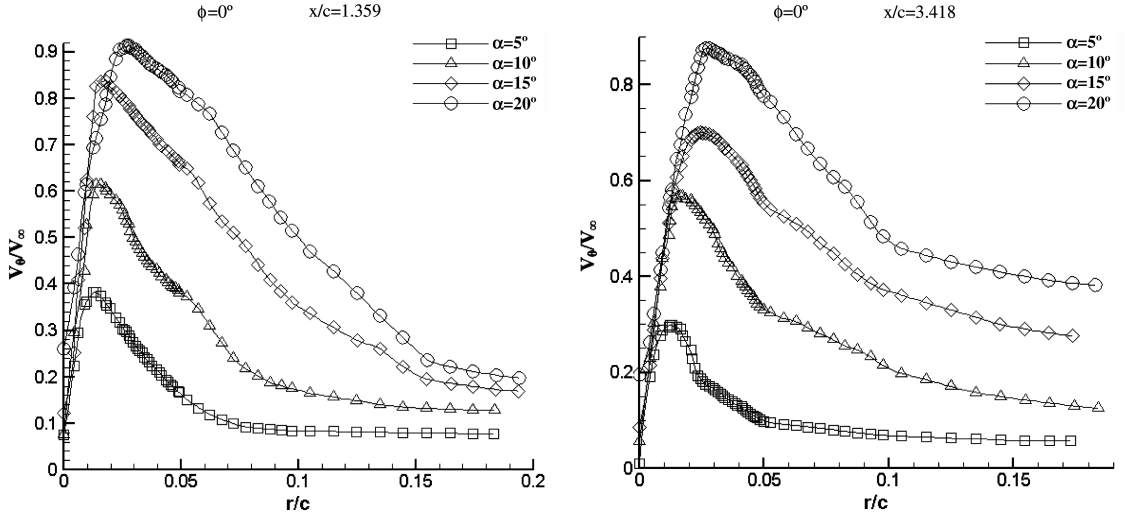

b) Tangential velocity distributions of a regular delta wing at ϕ=0°

Fig. 7 Nondimensional tangential velocity of tip vortices at $\phi = 0°$ at locations of $x/c = 1.359$ and 3.418 for a) reverse delta wing and b) regular delta wing.

C. Tangential Velocity

The tangential velocity around the vortex centerline, V_θ, is calculated as

$$v_\theta(r) = \frac{1}{k}\sum_{i=1}^{k} v_{\theta,i}(y,z)\Big|_{r=\sqrt{y^2+z^2}}$$

where k is the number of points for each radius; $r = \sqrt{y^2 + z^2}$; V_θ is normalized by the freestream velocity V_∞ and plotted versus the radial distance from the vortex centerline r, normalized by the chord length c; and r_c is defined as the core radius of the tip vortex, where maximum tangential velocity occurs. For $r < r_c$, the tangential velocity increases linearly and rapidly with radial distance until a maximum peak value. For $r > r_c$, the tangential velocity varies inversely with the radial distance r.

Figure 6a shows the tangential velocity distributions of an RDW vortex at $\alpha = 5°$. At a location of $x/c = 1.359$, the tangential velocity distributions exhibit double peaks. The tangential velocity distributions increase rapidly to a maximum value at the core , then vary inversely until a minimum value, and then increase gradually to a second peak at the outer region of the vortex. Since the tangential velocity magnitude is not sufficient for the vortex to completely roll up, as shown in Fig. 4a, the velocity vectors travel away from the vortex core to a region farther away. This gives rise to a second peak in the tangential velocity distributions at a location of $x/c = 1.359$, as shown in Fig. 6a. The second peak has a lower tangential velocity magnitude than the first peak.

Figure 6a shows a higher tangential velocity magnitude at a location of $x/c = 3.418$ for an RDW vortex at $\alpha = 5°$ and $\phi = -5°$, which may be due to the averaging of the PIV images. At a particular angle of attack, the difference in tangential velocity magnitudes for all the roll angles is very small, as shown in Figs. 6b–6d.

Figures 6b–6d show that the tangential velocity magnitude at a location of $x/c = 1.359$ is higher than at a location of $x/c = 3.418$ for both the RDW and the DW vortices, respectively. This is in agreement with the results shown in Figs. 4a–4d.

From Figs. 6a–6d, it can be seen that the maximum peak value of the tangential velocity is attained at $\phi = 0°$, the only exception being at a location of $x/c = 3.418$ for an RDW vortex at $\alpha = 5°$ and $\phi = -5°$, as shown in Fig. 6a. This suggests that the strength of the vortex is highest at $\phi = 0°$. A similar trend is shown for all studied angles of attack.

Figures 6a–6d yield that the tangential velocity distributions for DW vortices (Figs. 6c and 6d) are smoother than those for RDW vortices (Figs. 6a and 6b) and also show that the tangential velocity distributions at a location of $x/c = 3.418$ are smoother than at a location of $x/c = 1.359$. This can be linked to the roll-up of a vortex, whereby a vortex will have better roll-up at a farther downstream location, as shown in Figs. 4a–4d.

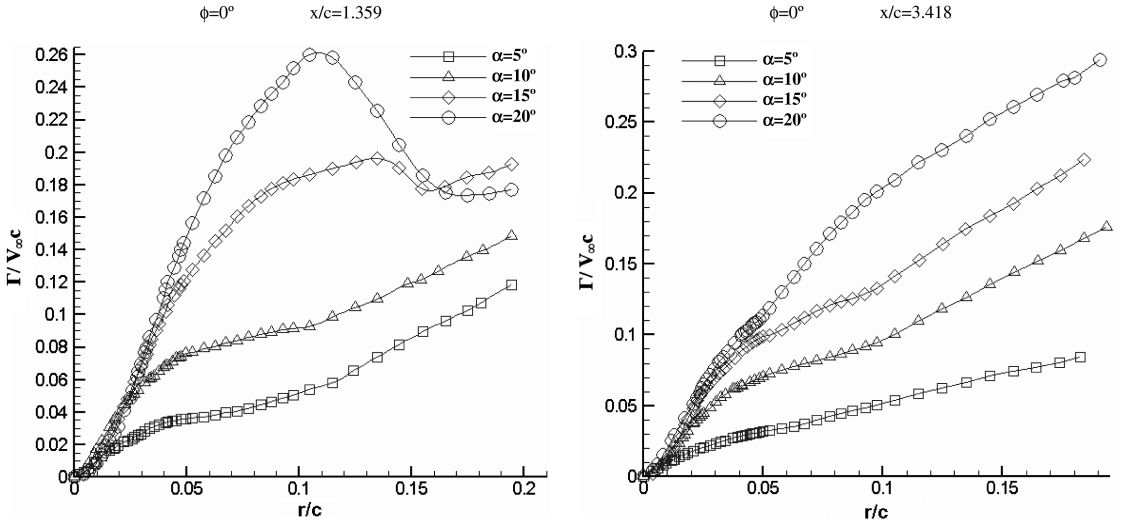

a) Circulation distributions of a reverse delta wing at ϕ=0°

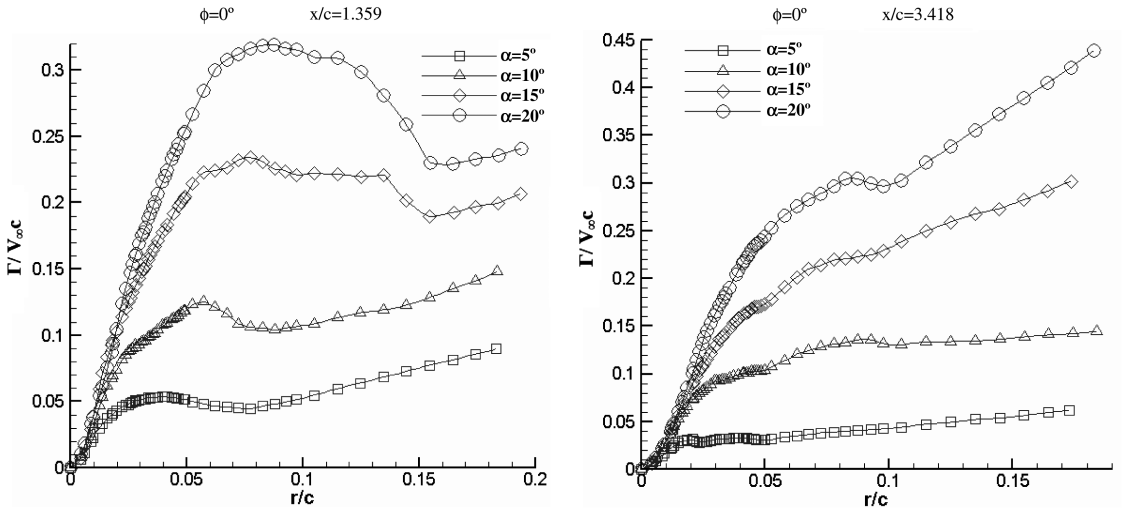

b) Circulation distributions of a regular delta wing at ϕ=0°

Fig. 8 Vortex strength $\Gamma(r)/V_\infty c$ versus radius r/c of tip vortex for various angles of attack at locations of $x/c = 1.359$ and 3.418 for a) reverse delta wing and b) regular delta wing.

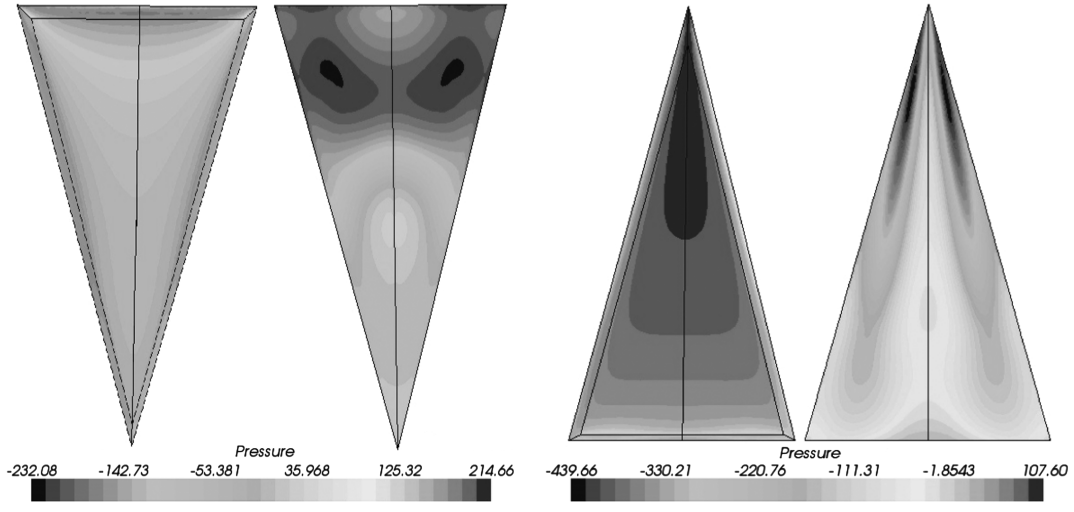

a) b)

Fig. 9 Pressure contours over the lower surface (left) and upper surface (right) at $\alpha = 30°$ and $\phi = 0°$ for a) reverse delta wing and b) regular delta wing. The legend refers to the gauge pressure.

This also highlights that a DW vortex has a better roll-up than an RDW vortex, because the tangential velocity distributions of DW vortices are smoother than those of RDW vortices.

Figures 7a and 7b show the tangential velocity distributions at $\phi = 0°$ for RDW and DW vortices, respectively. It can be concluded that as the angle of attack increases, the tangential velocity magnitude increases. Similar trends are achieved for all roll angles.

The r/c value from the origin to the peak of a tangential velocity distribution reveals the approximate size of the vortex core [16]. As angle of attack increases, the vortex core increases. This is in agreement with the results obtained in Figs. 4a–4d, whereby the vortex core size is seen to be increasing with an increase in angle of attack.

D. Circulation

The circular contours are centered about coordinates of maximum vorticity and plotted to estimate circulation. In Anderson [17] and Dobrev et. al. [18], circulation is estimated by

$$\Gamma = \int_A \zeta \, \mathrm{d}A$$

which in turn yields $\Gamma = 2\pi r v_\theta$ for an axisymmetric vortex that is treated as a cylinder. The circulation is normalized by $V_\infty c$.

Figures 8a and 8b show the circulation distributions for RDW and DW vortices, respectively. They reveal that the circulation increases for increasing angles of attack. The DW vortex was found to have a higher circulation distribution than that of an RDW vortex. At a location of $x/c = 1.359$, both the RDW and DW vortices show flatter circulation distributions, and at a location of $x/c = 3.418$, both the RDW and DW vortices show gradually increasing circulation distributions.

From Figs. 6a–6d, it can be noted that at a location of $x/c = 1.359$, both RDW and DW vortices' tangential velocity distributions flatten out at much lower tangential velocity magnitudes than those at a location of $x/c = 3.418$.

From Figs. 8a and 8b, at a location of $x/c = 1.359$, the distributions increase linearly and then flatten, because for $r > r_c$ the rate of change of V_θ/V_∞ with respect to r/c, as shown in Figs. 7a and 7b, is higher than at a location of $x/c = 3.418$. Thus, the magnitude of circulation varies only slightly, because circulation is directly related to r/c and V_θ. The product of r/c and V_θ does not continue to rise sharply and thus gives rise to flatter circulation distributions. From Figs. 8a and 8b the circulation distributions at a location of $x/c = 3.418$ increase gradually and do not show signs of flattening, due to a lower rate of change of V_θ/V_∞ with respect to r/c, as shown in Figs. 7a and 7b.

E. Simulation

Numerical simulations of the RDW and DW were carried out using CFD STAR-CCM software. Figure 9a highlights the pressure contours over an RDW. Both the lower (left) and upper (right) surfaces show that the pressure change occurs in a regular and linear fashion. Referring to the pressure coefficient legend, the upper surface (right image) of an RDW shows high changes in pressure gradient values near the trailing edges. This clearly highlights that strong pressure gradients exist at the trailing edges of an RDW.

In the case of a DW, as shown in Fig. 9b, the pressure change experienced by both the surfaces occurs in a nonlinear fashion. The upper surface (right image) of a DW shows high changes in pressure gradient values near the leading edges. This clearly highlights that strong pressure gradients are confined to the leading edges of a DW. The results shown in Fig. 9 are in agreement with Gerhardt's [7] study.

Figures 9a and 9b show that the pressure distribution over the lower surface of a DW has a higher average magnitude than the lower surface of an RDW and that the upper surface of a DW has a much lower average magnitude than the upper surface of an RDW. This higher difference in the pressure magnitudes of the lower and upper surfaces of a DW would yield a higher C_L than an RDW.

Figure 10a clearly shows how the flow and the vortices over the RDW behave, whereby the wing lies outside each tip vortices zone of influence. Figure 10b shows that the vortices over a DW are entirely over the wing, resulting in a higher C_L than a reverse delta wing. This is clearly evident from the results of a six-component force balance, as shown in Fig. 11a, which shows that a DW has a higher C_L than an RDW.

F. Aerodynamic Coefficients

The six-component force balance in the IIUM low-speed wind tunnel was used to compare the aerodynamic coefficients over an RDW with those over a DW, as shown in Fig. 11. Three dimensional flow boundary corrections were performed as stated in Barlow et al. [19], and the results obtained show a negligible change between the corrected and uncorrected values.

The reciprocal flow theorem for thin wings postulates that at sufficiently high Mach numbers, the lift-curve slope remains unchanged by flow reversal [7]. The same cannot be regarded for low-speed flow. At low speeds the lift-curve slope of a DW is not the same as the lift-curve slope of an RDW, as shown in Fig. 11a.

Figures 11a–11e show the comparison of six-component force balance results between an RDW and a DW at $\phi = 0°$. It reveals that an RDW has lower C_L and C_D than a DW. The lower C_D of an RDW results in a higher L/D ratio than that of a DW, as shown in Fig. 11e, whereas Fig. 11f shows the L/D ratio at $\phi = -20°$ and reveals that the L/D ratio of an RDW is lower than that of a DW. As the roll angle is varied, the trend for L/D ratio is not consistent, because the values of C_L and C_D do not show a consistent trend, but they do show a general trend whereby C_L and C_D of a DW are always higher than an RDW.

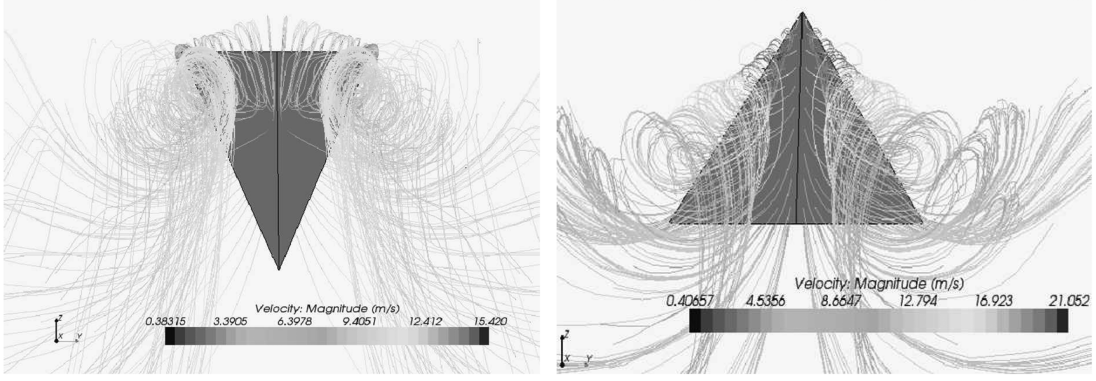

a) b)

Fig. 10 Streamlines over a) reverse delta wing and b) regular delta wing at $\alpha = 30°$ and $\phi = 0°$.

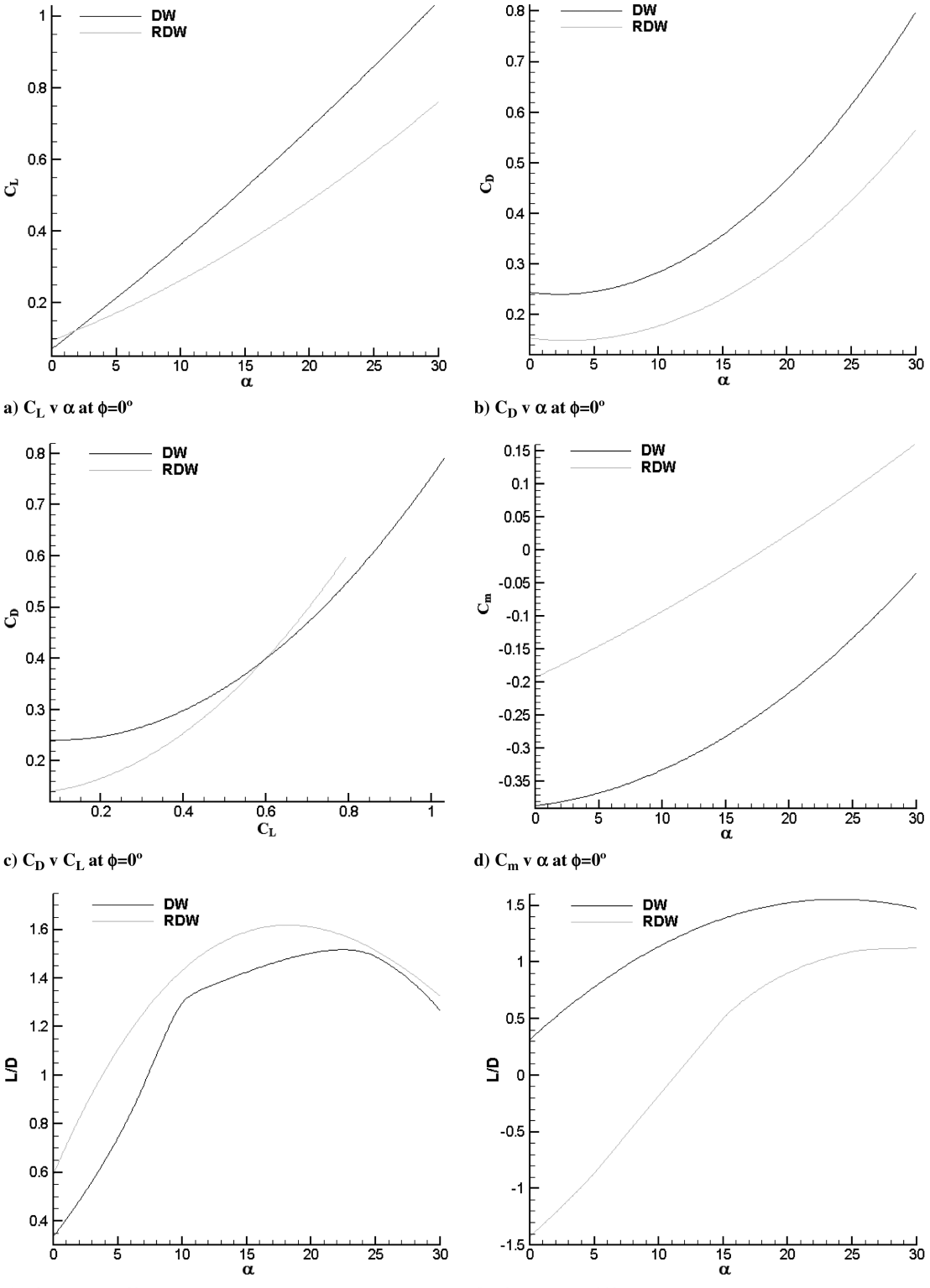

a) C_L v α at ϕ=0°

b) C_D v α at ϕ=0°

c) C_D v C_L at ϕ=0°

d) C_m v α at ϕ=0°

e) L/D v α at ϕ=0°

f) L/D v α at ϕ=20°

Fig. 11 Aerodynamic coefficients versus angle of attack α for an RDW and a DW.

IV. Conclusions

Reverse delta wingtip vortex structure and its characteristics were obtained in the IIUM low-speed closed-loop wind tunnel using particle image velocimetry. A comparison has been made with a regular delta wing of the same dimensions by reversing the flow. The vortex core radius grows with an increase in angle of attack for both the reverse delta wing and the regular delta wing. Tangential velocity and circulation distributions showed similar trends at different angles of attack and roll. Peak tangential velocity, vorticity, and circulation distributions showed a direct dependence on the angle of attack, whereby they increase with angle of attack. A reverse delta wing vortex at a particular angle of attack exhibited a lower magnitude of tangential velocity, circulation, and vorticity than a regular delta wing vortex. Since a reverse delta wing has low lift, it cannot be concluded whether the wake behind a reverse delta wing is less intense and less hazardous to trailing aircraft or not, because the wing area has to be increased to cater for same amount of payload. Thus, it is not yet clear whether stability problems of trailing aircraft could be reduced significantly if the lead aircraft has a reverse delta wing configuration. At low speeds, a reverse delta wing exhibits

approximately 26% lower C_L. Maximum circulation is obtained at $\alpha = 20^\circ$ for all cases, and hence maximum percent difference in circulation is calculated using data for $\alpha = 20^\circ$. At low speeds, a reverse delta wing exhibits approximately 18.75 and 33.33% lower circulation magnitude at locations of $x/c = 1.359$ and 3.418, respectively, than a regular delta wing. Results of the simulation of pressure contours are in agreement with Gerhardt's [7] study.

Acknowledgment

The authors would like to thank International Islamic University Malaysia for supporting this work through the Research Management Centre under the research grant no. EDW B 0905-294.

References

[1] Coustols, E., Jacquin, L., and Shrauf, G., "Status of Wake Vortex Alleviation in the Frame Work of European Collaboration: Validation Attempts Using Tests and CFD Results," *ECCOMAS CFD Conference*, Technical University of Delft, Delft, The Netherlands, 2006.

[2] Coustols, E., "An Overview of European Projects on Wake vortices," *Principles of Wake Vortex Alleviation Devices*, ONERA, Toulouse, France, 2006.

[3] Arndt, R. E. A., Arakeri, V. H., and Higuchi, H., "Some Observations of Tip Vortex Cavitation," *Journal of Fluid Mechanics*, Vol. 229, 1991, pp. 269–289. doi:10.1017/S0022112091003026

[4] Babie, B. M., and Nelson, R. C., "Flow Visualization Study of Far Field Wake Vortex Interactions," *11th International Symposium on Flow Visualization*, University of Notre Dame, Notre Dame, IN, Aug. 2004.

[5] "The X-29," NASA Dryden Flight Research Center, Rept. FS-2003-08-008-DFRC, Edwards AFB, CA, 2003, http://www.nasa.gov/centers/dryden/pdf/120266main_FS-008-DFRC.pdf [retrieved 10 March 2010].

[6] Taylor, M. J. H., *Brassey's World Aircraft & Systems Directory*, Brassey's, London, 1999, pp. 78–79.

[7] Gerhardt, H. A., "Supersonic Natural Laminar Flow Wing," Northrop Grumman Corp., Los Angeles, Patent No. 5538201, 1996.

[8] Norris, G., "Novel SST Configuration Revealed," *Flight International*, 23 Dec. 1998–5 Jan. 1999, p. 4; Flightglobal Archive, Aviation History, 1998, Paper 1998-3422, http://www.flightglobal.com/pdfarchive/view/1998/1998%20-%203422.html?tracked=1 [retrieved Sept. 2010].

[9] Elsayed, O. A., Asrar, W., and Omar, A. A., "Reverse Delta Wing Trailing Vortex Characteristics by Particle Image Velocimetry (PIV)," *3rd International Symposium on Advanced Fluid/Solid Science and Technology in Experimental Mechanics*, Tainan, Taiwan, 7–10 Dec. 2008.

[10] Srigrarom, S., "Effect of Delta Wing's Leading Edge Geometry to Vortex Breakdown," *15th Australasian Fluid Mechanics Conference*, Sydney, Australia, 13–17 Dec. 2004.

[11] Heron, I., "Vortex Burst Behaviour of a Dynamically Pitched Delta Wing Under the Influence of a Von Karman Vortex Sheet and Unsteady Freestream," Ph.D. Dissertation, Department of Aerospace Engineering, Wichita State University, Wichita, KS, Dec. 2007.

[12] Morton, S. A., "Detached Eddy Simulations of a 70 Degree Delta Wing in the ONERA F2 Wind Tunnel," *European Congress on Computational Methods in Applied Sciences and Engineering (ECCOMAS)*, 24–28 July 2004.

[13] Al-Garni, A. Z., Farooq, S., and Al-Garni, A. M., "Experimental and Numerical Investigation of 65-Deg Delta and 65/40-Deg Double-Delta Wings," *Journal of Aircraft*, Vol. 45, No. 1, 2008, pp. 71–76. doi:10.2514/1.20243

[14] Verhaagen, N. G., and Elsayed, M., "Leading Edge Radius Effects on 50 deg Delta Wing Flow," AIAA Paper 2009-0540, 2009.

[15] Figliola, R. S., and Beasley, D. E., *Theory and Design for Mechanical Measurements*, 2nd ed., Wiley, Singapore, 1995.

[16] Saffman, P. G., "The Number of Waves on Unstable Vortex Rings," *Journal of Fluid Mechanics*, Vol. 84, 1978, pp. 625–639. doi:10.1017/S0022112078000385

[17] Anderson, J. D., *Fundamentals of Aerodynamics*, 3rd ed., McGraw–Hill, Singapore, 2001, p. 215.

[18] Dobrev, I., Maalouf, B., Troldborg, N., and Massouh, F., "Investigation of the Wind Turbine Vortex Structure," *14th International Symposium on Applications of Laser Techniques to Fluid Mechanics*, Lisbon, Portugal, 7–10 July 2008.

[19] Barlow, J. B., Rae, W. H., and Pope, A., *Low-Speed Wind Tunnel Testing*, 3rd ed., Wiley, New York, 1999, pp. 367–427.